

Magnetic Superstructure and Metal-Insulator Transition in Mn-Substituted $\text{Sr}_3\text{Ru}_2\text{O}_7$

M.A. Hossain,^{1,2,*} B. Bohnenbuck,³ Y.-D. Chuang,² A.G. Cruz Gonzalez,² I. Zegkinoglou,³ M.W. Haverkort,³ J. Geck,¹ D.G. Hawthorn,¹ H.-H. Wu,⁴ C. Schüßler-Langeheine,⁴ R. Mathieu,⁵ Y. Tokura,⁵ S. Satow,⁶ H. Takagi,⁶ Y. Yoshida,⁷ J.D. Denlinger,² I.S. Elfimov,¹ Z. Hussain,² B. Keimer,³ G.A. Sawatzky,¹ and A. Damascelli^{1,†}

¹*Department of Physics & Astronomy, University of British Columbia, Vancouver, British Columbia V6T 1Z1, Canada*

²*Advanced Light Source, Lawrence Berkeley National Laboratory, Berkeley, California 94720, USA*

³*Max-Planck-Institut für Festkörperforschung, Heisenbergstraße 1, 70569 Stuttgart, Germany*

⁴*II. Physikalisches Institut, Universität zu Köln, Zùlpicher Straße 77, 50937 Köln, Germany*

⁵*Department of Applied Physics, University of Tokyo, Tokyo 113-8656, Japan*

⁶*Department of Advanced Materials Science, University of Tokyo, Kashiwa, Chiba 277-8581, Japan*

⁷*National Institute of Advanced Industrial Science and Technology (AIST), Tsukuba, 305-8568, Japan*

(Dated: Received May 7, 2009)

We present a temperature-dependent resonant elastic soft x-ray scattering (REXS) study of the metal-insulator transition in $\text{Sr}_3(\text{Ru}_{1-x}\text{Mn}_x)_2\text{O}_7$, performed at both Ru and Mn L -edges. Resonant magnetic superstructure reflections, which indicate an incipient instability of the parent compound, are detected below the transition. Based on modelling of the REXS intensity from randomly distributed Mn impurities, we establish the inhomogeneous nature of the metal-insulator transition, with an effective percolation threshold corresponding to an anomalously low $x \lesssim 0.05$ Mn substitution.

PACS numbers: 71.30.+h, 75.25.+z, 74.70.Pq

Electronic and lattice instabilities in strongly correlated electron systems give rise to many fascinating phenomena, such as for example various types of spin, charge, and orbital ordering. This is a common feature of many of the $3d$ transition-metal oxides, with the best-known examples including the stripe instability in the cuprate superconductors and the magnetic phase separation in manganites. Competing instabilities and ordering phenomena can also be found in the somewhat less correlated $4d$ transition-metal oxides, with the ruthenates being one of the most prominent families. $\text{Sr}_3\text{Ru}_2\text{O}_7$, which is the subject of this study, is known as a metal on the verge of ferromagnetism [1] due to the presence of strong ferromagnetic fluctuations. More recently, magnetic field tuned quantum criticality [2] and electronic nematic fluid behavior [3] have been proposed for this compound and associated with a metamagnetic transition. However, the deeper connection between these effects is still highly debated and its description will depend on a fuller understanding of the incipient instabilities in $\text{Sr}_3\text{Ru}_2\text{O}_7$.

Magnetic impurities such as Mn have been introduced in $\text{Sr}_3\text{Ru}_2\text{O}_7$ in an attempt to stabilize the magnetic order in the system [4]. It has been shown that due to the interplay between localized Mn $3d$ and delocalized Ru $4d$ - $\text{O}2p$ valence states, Mn impurities display an unusual crystal field level inversion already at room temperature [5]. Upon lowering the temperature, a metal-insulator phase transition has been observed for 5% Mn substitution at $T_c \simeq 50$ K, and at progressively higher T_c upon increasing the Mn concentration [4]. In this Letter, we investigate the nature of the low-temperature insulating phase of $\text{Sr}_3(\text{Ru}_{1-x}\text{Mn}_x)_2\text{O}_7$ and the role of Mn impurities using resonant elastic soft x-ray scattering (REXS). We will show that dilute Mn impurities not only induce long-range magnetic order but also provide a unique opportunity to probe the electronic instabilities in the parent compound and thereby reveal the mechanism behind the metal-insulator transition itself.

portunity to probe the electronic instabilities in the parent compound and thereby reveal the mechanism behind the metal-insulator transition itself.

A starting point for our REXS study has already been provided by previous neutron scattering work that detected $\mathbf{q} = (\frac{1}{4}, \frac{1}{4}, 0)$ and $(\frac{1}{4}, \frac{3}{4}, 0)$ superlattice peaks appearing below T_c for the 5% Mn system [4]. While this suggests the emergence of an electronic modulation and in particular of magnetic order, to specify its nature we need to establish if the modulation vector \mathbf{q} changes upon varying the Mn concentration beyond $x = 0.05$. In addition, to pinpoint the role of Mn impurities it is necessary to use an experimental tool that can probe Ru and Mn selectively. While neutron scattering experiments are sensitive to the average magnetic order, REXS can probe the order on Ru and Mn independently.

REXS is a relatively new spectroscopic technique to probe and study long-range charge/spin/orbital order in an element specific and direct way. REXS measurements were performed at beamlines 8.0.1 at ALS in Berkeley (Mn L -edges) and KMC-1 at BESSY in Berlin (Ru L -edges). In both cases we used a two-circle ultra-high-vacuum diffractometer in horizontal scattering geometry, with the incident photon beam polarized parallel to the diffraction plane (π). The scattered signal contained polarization components parallel (π') and perpendicular (σ') to the diffraction plane. $\text{Sr}_3(\text{Ru}_{1-x}\text{Mn}_x)_2\text{O}_7$ single crystals grown by the floating zone technique [4] were cut and polished along the (110) direction. The samples were mounted on cryogenic manipulators, allowing a cryostat polar angle rotation (θ) and also azimuthal rotation (ϕ) of the sample about the scattering vector, in the temperature range 20-300 K. Note that the diffraction peaks will be indexed with respect to the undistorted tetragonal $I4/mmm$ unit cell with axes along the RuO bond

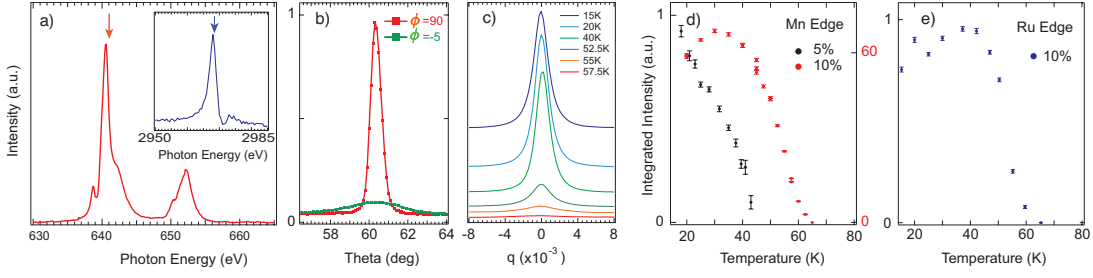


FIG. 1: (color online). (a) Mn and Ru (inset) resonance profile for the $(\frac{1}{4}, \frac{1}{4}, 0)$ superlattice diffraction peak measured at 20 K on $\text{Sr}_3(\text{Ru}_{1-x}\text{Mn}_x)_2\text{O}_7$ with $x=0.1$. The arrows at 641 and 2968 eV indicate the energies used in the REXS experiments. (b) 10 % Mn rocking curves for two different azimuthal angles ϕ measured at 641 eV and 20 K. (c) 10 % Mn $(\frac{1}{4} + \Delta q, \frac{1}{4} + \Delta q, 0)$ momentum scans at 641 eV for different temperatures. (d) Temperature dependence of the integrated intensity of the Mn-edge $(\frac{1}{4} + \Delta q, \frac{1}{4} + \Delta q, 0)$ momentum scans for $x=5$ and 10 % samples. (e) Same as (d), for the $x=10\%$ sample only, at the Ru edge.

directions ($a_0 = b_0 \simeq 3.9 \text{ \AA}$), while the magnetic and transport anisotropy will be discussed with reference to the 45° rotated and distorted orthorhombic $Bbcb$ unit cell of $\text{Sr}_3\text{Ru}_2\text{O}_7$ ($a^*, b^* \simeq 5.5 \text{ \AA}$) [6].

We performed REXS experiments on a range of Mn-substituted $\text{Sr}_3\text{Ru}_2\text{O}_7$ samples, at the Mn and Ru L -edges (for clarity, mostly data from 10 % Mn are shown in Fig. 1). For Mn concentration $x = 0.05$ and 0.1, this revealed a low-temperature structurally forbidden $\mathbf{q} = (\frac{1}{4}, \frac{1}{4}, 0)$ superlattice diffraction peak at the Mn L -edge. Similarly, experiments at the Ru L -edge on a 10 % sample detected $\mathbf{q} = (\frac{1}{4}, \frac{1}{4}, 0)$ and also $\mathbf{q} = (\frac{3}{4}, \frac{3}{4}, 0)$ reflections. Fig. 1(a) and its inset present the $(\frac{1}{4}, \frac{1}{4}, 0)$ resonance profile at $T=20 \text{ K}$, i.e. the energy dependence of this superlattice peak intensity at the Mn $L_{2,3}$ and Ru L_{2} -edges. Fig. 1(b) shows the Mn-edge $(\frac{1}{4}, \frac{1}{4}, 0)$ rocking curves at $T=20 \text{ K}$, i.e. the θ -angle dependence of the intensity at 641 eV for different azimuthal angles ϕ (see inset of Fig. 2 for the experimental geometry). Since the peak width in momentum is proportional to the inverse of the correlation length, the sharp $q_{x,y}$ dependence (θ scan at $\phi = 90^\circ$) and the broad response in q_z (θ scan at $\phi = -5^\circ$) indicate a two-dimensional order with weak correlation along the c -axis. Lastly, the structurally forbidden reflections are detected only below the DC transport metal-insulator T_c , with a progressively increasing strength upon reducing temperature and increasing Mn concentration. This is shown in Fig. 1(c) for the 10 % Mn-edge $(\frac{1}{4} + \Delta q, \frac{1}{4} + \Delta q, 0)$ scan, and in Fig. 1(d,e) for the Mn and Ru-edge integrated peak intensities (at 641 and 2968 eV, respectively).

Altogether, the results in Fig. 1 demonstrate that the metal-insulator transition is accompanied by a two-dimensional order with wavelength $2\sqrt{2}a_0$ and modulation vector \mathbf{q} along the diagonal of the $I4/mmm$ zone. The order is predominantly electronic and not structural (we did not observe corresponding superlattice reflections in non-resonant low-temperature x-ray diffraction), nor associated with the spatial ordering of the Mn impurities as evidenced by the doping independence of \mathbf{q} . The nature of this electronic order, i.e. spin/charge/orbital,

can be further clarified by the detailed azimuthal-angle dependence of the integrated intensity of the Ru and Mn-edge $(\frac{1}{4}, \frac{1}{4}, 0)$ peaks. The results for the 10 % Mn system are presented in Fig. 2, together with a theoretical angle dependence calculated for pure spin order [7], with spins parallel to the c -axis. The agreement between measured and calculated azimuthal dependence implies the primarily magnetic nature of the ordering, with average spin direction along the c -axis at both Ru and Mn sites.

To specify the exact pattern of the spin order, we should note that in addition to the above mentioned forbidden superlattice peaks, also a $\mathbf{q} = (\frac{1}{4}, \frac{5}{4}, 0)$ reflection was observed in our neutron scattering study on the $x=0.05$ material [8]. Instead, no $\mathbf{q} = (\frac{1}{2}, \frac{1}{2}, 0)$ reflection was detected with either neutron or REXS at the Ru edge (at the Mn edge this \mathbf{q} value cannot be reached). These results enforce a very strong constraint on the possible spin texture but still allow for more than one compatible

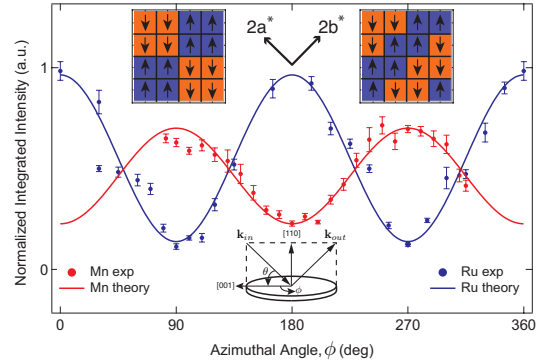


FIG. 2: (color online). Azimuthal-angle dependence of the $(\frac{1}{4} + \Delta q, \frac{1}{4} + \Delta q, 0)$ momentum scan integrated intensity, at the Ru and Mn edge for the $x=0.1$ sample. Both datasets are fitted to the formula $I_{(\frac{1}{4}, \frac{1}{4}, 0)}^{total} = I_{(\frac{1}{4}, \frac{1}{4}, 0)}^{\pi \rightarrow \sigma'} + I_{(\frac{1}{4}, \frac{1}{4}, 0)}^{\pi \rightarrow \pi'} \propto |\cos \theta \cos \phi|^2 + |\sin 2\theta \sin \phi|^2$. Due to the different Mn and Ru scattering angles ($\theta_{Mn} = 61.6^\circ$; $\theta_{Ru} = 10.9^\circ$), the ratio between $(\pi \rightarrow \sigma')$ and $(\pi \rightarrow \pi')$ scattering signals is also different and the maximum intensity position is shifted by 90° in ϕ . The experimental geometry and the two highest symmetry spin patterns consistent with the data are also shown.

spin pattern. Among those, the most significant are the two highest symmetry ones, which due to the presence of domains (more below) would give rise to identical REXS patterns: a *checkerboard* antiferromagnetic ordering of square blocks of four parallel spins (Fig. 2, left inset); alternatively, an antiferromagnetic alternation of ferromagnetic *zigzag stripes* aligned diagonally with respect to the tetragonal $I4/mmm$ zone (Fig. 2, right inset). While the checkerboard pattern is isotropic with respect to the crystallographic a^* and b^* axes of the $Bbcb$ orthorhombic zone, the zigzag stripe pattern is not. Since this electronic anisotropy is appealing in relation to the reports of a nematic fluid phase in $\text{Sr}_3\text{Ru}_2\text{O}_7$ with a^*-b^* resistive anisotropy in an applied magnetic field [3, 9], let us continue by focusing on the zigzag stripe order; note, however, that the following discussion on the nature of the metal-insulator transition is independent of this choice.

Because of their coincidence in temperature, it seems natural to associate the metal-insulator transition with the onset of magnetic order induced by the Mn impurities. To further our understanding of the mechanism of the metal-insulator transition, we have studied the doping and temperature dependence of the width and intensity of the Mn-edge momentum scans, which provide an estimate of the magnetic-order correlation length and of the fraction of participating Mn impurities. Fig. 3(a) presents a comparison of the Mn-edge ($\frac{1}{4} + \Delta q, \frac{1}{4} + \Delta q, 0$) momentum scans at 20 K for $x = 0.05$ and 0.1. As evidenced by the combination of normalized (main panel) and raw data (inset), both the integrated intensity and peak width are strongly enhanced (by factors of 10 and 4, respectively) upon increasing x from 5 to 10%. The detailed temperature dependence of the Mn-edge correlation length, defined as the inverse of the full-width half maximum (FWHM) of the momentum scans, is shown in Fig. 3(b) for both samples (similar correlation length results were obtained at the Ru-edge).

To start modelling this behavior, we should note that only the magnetically correlated Mn impurities contribute to the $(\frac{1}{4}, \frac{1}{4}, 0)$ scattering intensity at the Mn L -edge; calculations assuming a random distribution of Mn sites show that if 100% of the Mn impurities took part in the long-range spin order, as Mn doping is increased from 5 to 10% the diffraction peak integrated intensity should increase by a factor of about 4, i.e. nearly quadratically in the number of scattering centers [10]. The observed 10-fold increase implies that a much smaller fraction of the Mn moments are correlated for $x = 0.05$ and suggests the following scenario for the emergence of long-range magnetic order. At a sufficiently low temperature, each Mn impurity surrounds itself by a two-dimensional spin-ordered island, within the metallic RuO_2 plane. When these islands begin to overlap, the RuO-mediated exchange interaction can energetically favor a coherent spin arrangement between the islands and, as a result, the Mn impurities will interfere constructively. In the dilute 5%

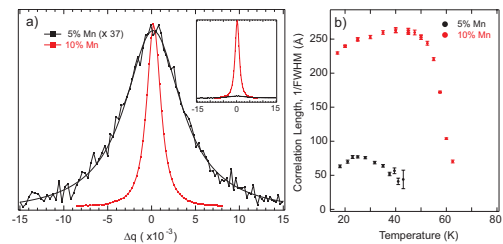


FIG. 3: (color online). (a) Normalized Mn-edge ($\frac{1}{4} + \Delta q, \frac{1}{4} + \Delta q, 0$) momentum scans at 20 K for 5% (with Lorentzian fit) and 10% Mn concentration; raw data are shown in the inset. (b) Inverse FWHM of the momentum scans vs. temperature.

Mn regime, there are isolated Mn impurities whose spins are not participating in the order and will not contribute to the superlattice diffraction peak intensity; at 10% Mn concentration, however, there are statistically hardly any isolated Mn atoms and hence almost all them will contribute. As experimentally observed, the diffraction peak intensity would increase much faster than quadratically with increasing x .

It might appear surprising that a REXS signal is obtained from dilute, randomly distributed Mn impurities. One should realize, however, that constructive interference is dependent not on the spatial location of the impurities, provided that the Mn atoms occupy substitutional Ru sites, but rather on the proper phase relation between their magnetic moments. This can be demonstrated with a simulation based on the correlation lengths obtained from the inverse of the FWHM of the experimental momentum scans (~ 55 and 235 \AA for 5 and 10% Mn concentration, respectively, at 20 K). Fig. 4(a) presents a 40×40 RuO_2 lattice in real space, with 5% Mn sites each inducing a 4×4 unit of the zigzag stripe pattern (the simulation would identically apply to the case of the checkerboard ordering). Here, no correlation between the Mn spins has been imposed. As in Fig. 2, blue and red squares in Fig. 4(a) represent up and down spins along the c -axis, while the white patches are regions of the RuO_2 lattice where no magnetism has been induced [the position of the Mn impurities and their corresponding spins are shown in Fig. 4(b)]. Due to the lack of correlation between the Mn spins, the Mn-edge ($\pm \frac{1}{4}, \pm \frac{1}{4}, 0$) peaks are extremely broad and weak, buried in the noisy background, as shown by the reciprocal space map of the scattering intensity in Fig. 4(c). The situation is very different for correlated Mn spins, as shown in Fig. 4(d,e,f) which presents the same sequence as panels (a,b,c), still for $x = 5\%$, but for an average cluster size of 55 \AA (~ 13 lattice spacing) as observed experimentally. The superlattice ($\pm \frac{1}{4}, \pm \frac{1}{4}, 0$) peaks are clearly discernible above the noise in Fig. 4(f). Note that this particular spin pattern also gives rise to $(\frac{2n+1}{4}, \frac{2n+1}{4}, 0)$ diffraction peaks, with n being an integer, but for the present discussion it is sufficient to restrict the field of view to $q_x, q_y = \pm 0.5 \pi/a_0$. For $x = 10\%$ and $\sim 235 \text{ \AA}$ magnetic islands (~ 57 lattice

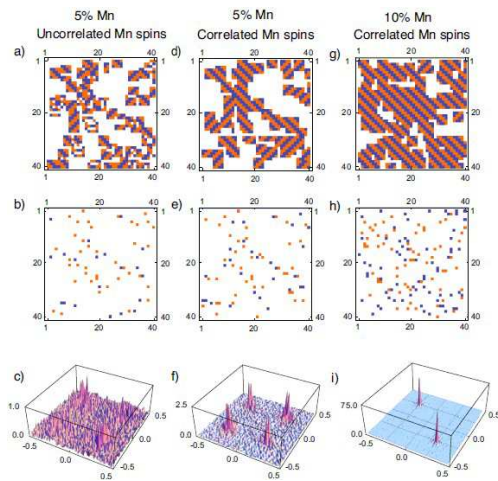


FIG. 4: (color online). (a,d,g) Spin-ordered islands in the RuO_2 plane for various Mn contents and spin correlations: (a) 5% Mn, uncorrelated Mn spins; (d) 5% Mn, correlated Mn spins; (g) 10% Mn, correlated Mn spins. (b,e,h) Corresponding location of Mn impurities with up/down (blue/red) spins. (c,f,i) Reciprocal space map of the Mn scattering intensity generated by averaging over 200 random Mn-impurity distributions, of the kind in (b,e,h), to reduce noise.

spacing), we can observe in Fig. 4(g,h,i) sharp diffraction spots with a peak height 30 times that of $x = 5\%$, in good agreement with the experimentally observed ~ 37 -fold increase (Fig. 3a). We should also note that $(\frac{1}{4}, -\frac{1}{4}, 0)$ and $(-\frac{1}{4}, \frac{1}{4}, 0)$ peaks are absent because the domain size is now larger than the lattice cell used for the simulation; in the real experiments they would be still visible.

We can now summarize our findings and try to establish a connection between long-range spin order and metal-insulator transition in $\text{Sr}_3(\text{Ru}_{1-x}\text{Mn}_x)_2\text{O}_7$, and possibly the magnetic fluctuations and nematic fluid behavior of the parent compound. Since $\text{Sr}_3\text{Ru}_2\text{O}_7$ does not show any long-range magnetic order, it is clear that the latter is induced by the $S=2$, $3d$ - Mn^{3+} impurities [4, 5]. Nevertheless, the ordering is independent of the precise 5-10% Mn concentration, suggesting that the role of Mn is primarily that of triggering and/or stabilizing an instability incipient in the parent compound. Indeed, strong two-dimensional spin fluctuations have been observed in $\text{Sr}_3\text{Ru}_2\text{O}_7$ in zero field, which appear to cross over from ferro to antiferromagnetic upon reducing the temperature below 20 K [11]; and also a momentum-dependent spin anisotropy induced by spin-orbit coupling should be expected, as in Sr_2RuO_4 [12]. For both checkerboard and zigzag stripe spin patterns, the insulating behavior would result from the interaction of the propagating carriers with the ordered spin background. Note, however, that the zigzag stripe order would exhibit a marked transport anisotropy even in the absence of any applied field, with high and low conductivity behavior, respectively, along and perpendicular to the ferromagnetic stripes. In this latter case the macroscopic metal-insulator transi-

tion would thus depend on the formation of magnetic domains with different orientation. One might speculate that the transport anisotropy expected for a single zigzag stripe domain in $\text{Sr}_3(\text{Ru}_{1-x}\text{Mn}_x)_2\text{O}_7$, and the one detected in the parent compound in magnetic fields [3], could be fingerprints of the same nematic fluid instability [9]; this however will require further scrutiny.

It should be emphasized that $\text{Sr}_3(\text{Ru}_{1-x}\text{Mn}_x)_2\text{O}_7$ in the dilute Mn substitution regime provides a unique opportunity to study with great accuracy the role of impurities and disorder in inducing phase separation, percolative, and glassy behavior in the general class of correlated oxides. For instance, it is interesting to note that the effective percolation threshold is achieved at $\lesssim 5\%$ Mn concentration [4]; in terms of magnetically correlated sites, as shown in Fig. 4(a,d) this corresponds to 50.2% of the RuO_2 plane, thus remarkably close to the threshold for classical metallic percolation on a square lattice which is suppressed at a 50% mixture of metallic and insulating bonds [13]. Furthermore, the non-monotonic temperature dependence of the correlation length presented in Fig. 3(b) has also been seen in reentrant spin glasses, due to the interplay of competing interactions and disorder [14, 15]. Finally, speculating on the much higher resonant enhancement observed at the Mn as compared to the Ru absorption edge (an at-least 36-fold enhancement should be expected due to the cross-section difference between $2p$ - $3d$ and $2p$ - $4d$ excitations), one might imagine using random impurities as a highly sensitive probe of spin/charge/orbital order of a host system that is difficult to access via the majority lattice population.

We thank M.Z. Hasan for the use of the ALS scattering chamber. This work is supported by ALS (M.A.H), Sloan Foundation (A.D.), CRC Program (A.D., G.A.S.), NSERC, CFI, CIFAR, and BCSI. ALS is supported by the U.S. DOE Contract No. DE-AC02-05CH11231.

* Electronic address: hossain@slac.stanford.edu

† Electronic address: damascelli@physics.ubc.ca

- [1] S.I. Ikeda *et al.*, Phys. Rev. B **62**, R6089 (2000).
- [2] S.A. Grigera *et al.*, Science **294**, 329 (2001).
- [3] R.A. Borzi *et al.*, Science **315**, 214 (2007).
- [4] R. Mathieu *et al.*, Phys. Rev. B **72**, 092404 (2005).
- [5] M.A. Hossain *et al.*, Phys. Rev. Lett. **101**, 016404 (2008).
- [6] H. Shaked *et al.*, J. Solid State Chem. **154**, 361 (2000).
- [7] J.P. Hill and D.F. McMorrow, Acta Crystallogr., Sect. C: Found. Crystallogr. **52**, 236 (1996).
- [8] R. Mathieu, T. Arima, and Y. Tokura (unpublished).
- [9] S. Raghu *et al.*, arXiv:0902.1336 (2009).
- [10] M.W. Haverkort *et al.* (unpublished).
- [11] L. Capogna *et al.*, Phys. Rev. B **67**, 012504 (2003).
- [12] M.W. Haverkort *et al.*, Phys. Rev. Lett. **101**, 026406 (2008).
- [13] S. Kirkpatrick, Rev. Mod. Phys. **45**, 574 (1973).
- [14] H. Maletta *et al.*, Phys. Rev. Lett. **48**, 1490 (1982).
- [15] G. Aeppli *et al.*, Phys. Rev. B **28**, 5160 (1983).